Spin-dimerization in rare-earth substituted La_2RuO_5

S. Riegg[1,a], A. Günther[1], H.-A. Krug von Nidda[1], M.V. Eremin[2], A. Reller[3], A. Loidl[1], and S.G. Ebbinghaus[4]

[1] Experimental Physics V, Center for Electronic Correlations and Magnetism, University of Augsburg, 86159 Augsburg, Germany
[2] Kazan Federal University, 420008 Kazan, Russian Federation
[3] Resource Strategy, University of Augsburg, 86159 Augsburg, Germany
[4] Solid State Chemistry, Martin-Luther University Halle-Wittenberg, 06099 Halle, Germany

Abstract. The Ru-Ru spin-singlet formation in $La_{2-x}Ln_xRuO_5$ (Ln = Pr, Nd, Sm, Gd, Dy) was investigated by measurements of the specific heat and magnetic susceptibility. After subtraction of the lattice contribution from the specific heat (C_p), similar excess entropy values were obtained for all compounds. These entropies can be explained by the formation of antiferromagnetic Ru-spin dimers at low temperatures and provide a lower estimate for the intradimer exchange strength. Pronounced changes in the transition temperatures and a broadening of the corresponding peak in C_p were observed. These changes depend on the rare-earth element and are due to local structural changes and heterogeneities caused by the substitution. The magnetic susceptibilities can be described by the sum of a rare-earth paramagnetic moment and the susceptibility of the unsubstituted La_2RuO_5. Density functional theory (DFT) calculations were performed for various compounds to investigate the origin of the magnetic transition and the relationship between structural changes and the spin-dimerization temperature. The combination of the present results with previous structural investigations supports the model of a spin-pairing of the Ru moments which occurs as a reason of the structural phase transition in $La_{2-x}Ln_xRuO_5$.

1 Introduction

Rare earth containing ruthenium-oxides often exhibit quite different magnetic transition temperatures of the respective electronic subsystems (based on the d- and f-electrons) caused by rather different strenghts of the corresponding exchange interactions. For example, the double perovskites Ln_2LiRuO_6 show an almost independent ordering of the Ru^{5+} and the Ln^{3+} magnetic moments, however the existence of a weak coupling between these ions has also been reported [1]. Another example is Sr_2RuGdO_6, in which an independent ordering of the Ru and the Gd sublattices was observed below 33 K and 2 K, respectively, although Gd and Ru are both occupying the B-sites of the compound [2]. The layered $Nd_2BaLiRuO_7$, an $n = 2$ Ruddlesden-Popper phase, shows an independent antiferromagnetic ordering of Ru^{5+} (T_N = 32 K) and Nd^{3+} moments (T_N = 2 K), respectively, within the layers [3]. In contrast, for Ln_2RuO_5 (Ln = Pr, Nd, Sm, Gd, Tb)[1] a magnetic ordering below 24 K involving both Ru- and Ln-moments has been observed [5]. However, none of these examples undergoes a combined structural and magnetic phase transition as it was observed for La_2RuO_5 and for rare-earth substituted $La_{2-x}Ln_xRuO_5$ [6–8]. La_2RuO_5 shows a dimerization of the spin moments driven by structural changes at 161 K which is a surprisingly high temperature for an effectively two dimensional (2D) system [6,9–12].

La_2RuO_5 possesses a layered crystal structure with $LaRuO_4$ perovskite-like layers and buckled LaO-layers alternating along the a-axis as depicted in Figure 1 and described in more detail in references [13,14]. In La_2RuO_5 the phase transitions observed at 161 K affects structure, magnetic properties and electrical conductivity [6,15]. The high-temperature (ht-) phase is characterized by a monoclinic symmetry (space group $P2_1/c$, no. 14), a paramagnetic behavior in accordance with the $S = 1$ spin moments of the Ru^{4+} ions, and a band gap of roughly 0.15(5) eV [6]. In contrast, the low-temperature (lt-) phase has a triclinic symmetry (space group $P\bar{1}$, no. 2), the magnetic susceptibility is strongly reduced to roughly 10^{-4} emu/mol, and the band gap increases to 0.21(5) eV [6]. For the rare-earth substituted $La_{2-x}Ln_xRuO_5$ (Ln = Pr, Nd, Sm, Gd, Dy) very similar structural and magnetic properties were observed [8]. These will be further investigated and discussed in this publication.

Spin polarized DFT calculations using an augmented spherical wave (ASW) approach revealed an

[a] e-mail: stefan.riegg@physik.uni-augsburg.de

[1] Despite their identical sum formula, these Ln_2RuO_5 rare-earth ruthenates possess a completely different structure than La_2RuO_5. The structure of Ln_2RuO_5 is orthorhombic and related to Y_2TiO_5 [4].

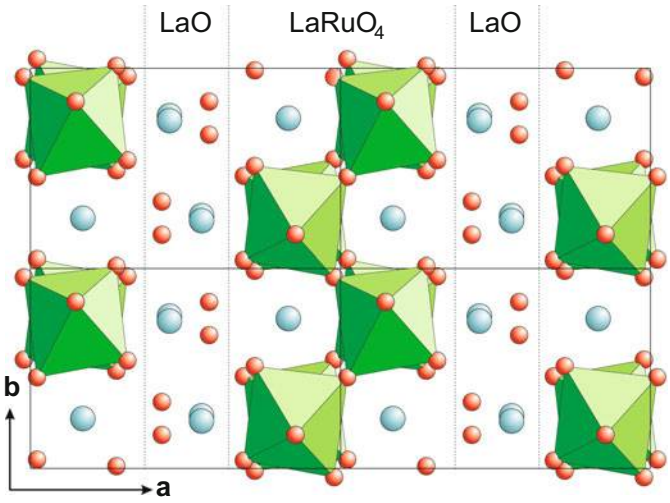

Fig. 1. (Color online) Crystal structure of $La_{2-x}Ln_xRuO_5$ (2×2 unit cells) viewed along the c-axis. La/Ln ions are represented by large turquoise spheres, oxygen by small red spheres and the RuO_6 octahedra are drawn in light green. The alternating layering of LaO and $LaRuO_4$ along the a-axis is indicated by dotted lines.

antiferromagnetic pairwise ordering of the $S = 1$ spin moments leading to an almost complete depression of the macroscopic magnetic susceptibility [14,16,17]. The same result was obtained by a second research group using LSDA+U calculations[2] in combination with X-ray absorption measurements on single crystals [10]. From these findings, a spin-ladder arrangement of Ru-Ru dimers as rungs was derived reflecting the strong anisotropy of the obtained exchange paths J_i.

Lately, we compared the experimental magnetic transition with calculations based on a model of $S = 1$ dimers, which are weakly interacting with the surrounding dimers in a spin ladder similar to Samulon et al. [18]. As an alternative model we additionally studied the interaction strengths of a 2D Heisenberg model. This model may be applied because of the square Ru-lattice present in the $LaRuO_4$-layers of the layered crystal structure. The respective coupling constants were obtained from fits of the high temperature region [12]. It turned out that none of the models was able to describe the experimental data at low temperatures since the observed transition temperature is much higher than predicted by both models. This result corroborates the importance of the structural changes occuring at the transition temperature.

We recently managed to partly substitute La by other lanthanides (Pr, Nd, Sm, Gd, Dy) leading to samples with the composition $La_{2-x}Ln_xRuO_5$, which were used to study the influence of structural changes and magnetic interactions on the magneto-structural phase transition [7,8]. The most important result was a shift of the transition temperature to lower values with increasing substitution level. This temperature shift can be explained by a broadening of the Ru bands close to the Fermi energy caused by stronger hybridization. The magnetic susceptibility above the transition temperature can be well described by the sum of the Ru^{4+} and Ln^{3+} moments forming two weakly interacting magnetic subsystems [8]. It was found that the maximum substitution level x depends on the size of the respective rare earth. This effect can be explained by the structural stress introduced by the size mismatch between La^{3+} and Ln^{3+} [8].

In this work the examination of magnetic properties is extended to the low-temperature region. In addition, the phase transition in $La_{2-x}Ln_xRuO_5$ is studied by specific heat measurements to investigate the effect of the different substitution levels and of the different rare-earth elements on the Ru-spin dimerization. The compounds with the highest possible degree of substitution for each rare earth were chosen. The results are compared with magnetic susceptibility data. The ordering of the Ru^{4+} moments is furthermore studied by DFT calculations using LSDA.

2 Experimental details and DFT calculation settings

2.1 Experimental

Polycrystalline samples of $La_{2-x}Ln_xRuO_5$ were obtained by a soft-chemistry reaction. This preparation route bases on the thermal decomposition of citrate precursors and is described in detail elsewhere [8].

The specific heat at constant pressure C_p was measured in the range 1.8 K $\leq T \leq$ 300 K using a physical property measurement system (Quantum Design PPMS). In the range of the phase transition ($\pm$15 K) as well as below 30 K the specific heat was recorded in steps of 0.2 K. Except for these regions, the temperature was changed in steps of 1 K. Pellets with 3 mm diameter were pressed from a mixture of approximately 10 mg of the sample powder and 2 mg of polyvinyl alcohol (PVA). The contribution of PVA was subtracted from the experimental data. The fit of the lattice contribution was performed with the program Mathematica 7 applying an Einstein-Debye 3D-phonon model.

The magnetic susceptibilities $\chi = M/H$ were investigated using a superconducting quantum interference device (SQUID) magnetometer (Quantum Design MPMS-XL) between 2 K and 400 K. Field cooled conditions with $H = 1000$ Oe were applied for all measurements. The powder samples were enclosed in gel capsules, whose small contribution to the measured susceptibility was taken into account by a temperature independent χ_0 parameter in the data fitting procedure [8]. Additional magnetization measurements were carried out in the PPMS in the range 50 K to 250 K with external fields between $H = 5$ kOe and 80 kOe.

2.2 DFT calculation settings

Band structure calculations were performed with the full-potential local-orbital minimum base code (FPLO 7.00-28) [19,20]. Structural information for the DFT calculations were taken from Rietveld-refinements of X-ray and

[2] Local Spin Density Approximation including an on-site repulsion Hubbard U term.

neutron powder diffraction patterns [8]. The symmetry was lowered to P1 for both the ht- and lt-phase to replace single La ions by Ln and to study the magnetic mutual interaction of the Ru ions applying LSDA. The number of k points was adapted to the reciprocal unit cell axis lengths and set to $3 \times 6 \times 4$. These numbers were chosen considering the upper limit of matrix elements available in the program code. A scalar relativistic setting was applied for the spin polarized calculations. Convergence criteria concerning the minimization of changes of the atomic density and total energy were used. Several iterations of the modelling had to be performed using the previously obtained results as starting parameters.

To investigate the effect of the rare-earth substitution, one, two, and three La-ions were replaced by Pr ions, respectively, reflecting the substitution levels $x = 0.25$, 0.50, and 0.75. Different arrangements of Pr in the crystal lattice were tested. The lowest total energy was achieved for the different substitutions as follows: for $x = 0.25$ when the single rare-earth ion was placed in the LaO layer, for $x = 0.50$ when the two Pr ions were divided to occupy both layers, and for $x = 0.75$ one Ln had to be placed in the $LaRuO_4$-layer and two in the LaO-layer. In the ht-modifications the same lanthanide-ion distribution had to be applied to obtain minima in total energy. These lanthanide-ion distributions are in accordance with neutron-diffraction results of Pr substituted compounds [8] and EXAFS investigations [21]. Studies of the antiferromagnetic arrangement in the lt-phase were performed for Pr substituted compounds with the same rare-earth distribution scheme like in the ht-phase.

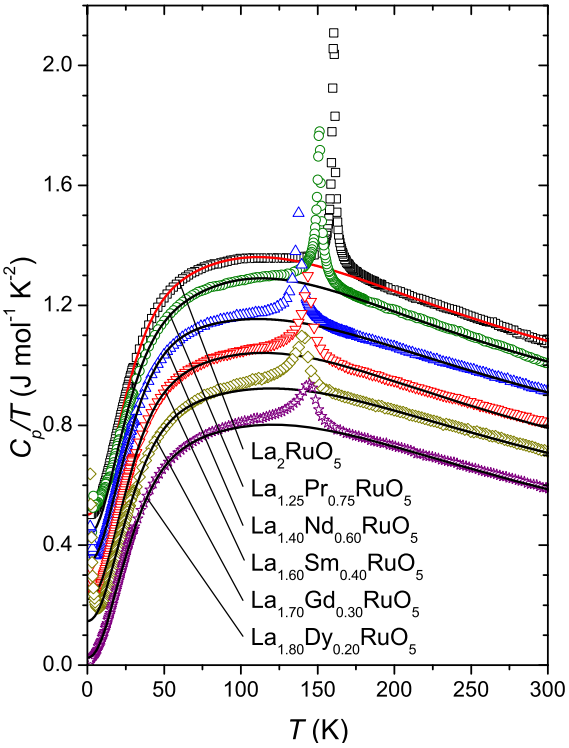

Fig. 2. (Color online) Temperature dependence of the specific heat in the representation C_p/T vs. T for La_2RuO_5 and $La_{2-x}Ln_xRuO_5$ with the highest available substitution level for each rare earth (symbols). For clarity the curves were shifted. The solid lines mark the Einstein-Debye fits. For more details see text.

3 Experimental results

3.1 Specific heat

The specific heat was measured for undoped La_2RuO_5 and for the rare-earth substituted compounds with the highest achievable substitution level of each rare-earth element. The measured curves of C_p/T are depicted in Figure 2, shifted in equidistant steps for clarity. All samples provide very similar heat capacities and reach a value of $C_p \approx 180$ J mol^{-1} K^{-1} at 300 K. Thus the expected Dulong-Petit limit $C_p = 3z \times \mathrm{R} \approx 199.54$ J mol^{-1} K^{-1} (z is the number of atoms per f.u. and R is the gas constant) is not yet reached at room temperature. A peak between 130 K and 170 K was observed for all samples mirroring the magneto-structural phase transition. The peaks show an increasing asymmetric broadening with increasing atomic number of the lanthanide.

The lattice contribution was fitted using an Einstein-Debye model with one Debye (Θ_D) and seven Einstein (Θ_E) terms according to the eight atoms per formula unit. The fitting was carried out according to the procedure described in references [22,23]. To reduce the degrees of freedom a weighting scheme $1 \times \Theta_D + 1 \times \Theta_{E1} + 1 \times \Theta_{E2} + 1 \times \Theta_{E3} + 4 \times \Theta_{E4}$ was applied taking into account the alternating LaO and $LaRuO_4$ layers. Thus each crystallographic site is described by a single term except the contribution of the four oxygen atoms in the $LaRuO_4$ layers, which were grouped to a single quadruple weighted term Θ_{E4}. The resulting Debye- and Einstein-temperatures are listed in Table 1. The individual temperatures are increasing from La_2RuO_5 to $La_{1.8}Dy_{0.2}RuO_5$ following the atomic number and in turn the weight of the rare-earth element. This behavior also reflects the increasing rigidity of the crystal lattice according to the smaller unit-cell volumes, which were observed for increasing substitution level and decreasing size of the lanthanide ion [8].

For the lanthanides the influence of the crystal-field excitations is increasing the heat capacity below roughly 15 K as shown in Figure 3 using a representation C_p/T^3 vs. T according to a Debye T^3 model. A logarithmic scale for the ordinate axis was chosen to increase clarity in the low-temperature range. The rise observed for the rare-earth substituted samples can be described as Schottky-type anomaly caused by crystal-field splitting of the $4f$ levels [22,24]. The crystal-field Schottky anomaly is proportional to T^{-2} (for $T \gg \Delta_{CF}$) in C_p [25]. Correspondingly, this behavior is proportional to T^{-5} in C_p/T^3, which is marked by the solid line in Figure 3. The expected T^{-5} behavior is observed for the Nd, Sm, and Gd substituted samples, which could even be improved by subtraction of the La_2RuO_5 experimental data. For $La_{1.25}Pr_{0.75}RuO_5$ the data below 4 K seem to be unreliable and for $La_{1.8}Dy_{0.2}RuO_5$ the crystal-field excitations

Table 1. Results of the heat-capacity fits of $La_{2-x}Ln_xRuO_5$ (see text for details). The magnetic entropy S_{mag} was calculated by the integration of C_p/T after the subtraction of the lattice contribution.

Sample	Θ_D (K)	Θ_{E1} (K)	Θ_{E2} (K)	Θ_{E3} (K)	Θ_{E4} (K)	S_{mag} $\left(\frac{\mathrm{J}}{\mathrm{mol\ K}}\right)$
La_2RuO_5 [12]	132	175	217	325	520	4.2(3)
$La_{1.25}Pr_{0.75}RuO_5$	132	175	222	335	515	3.9(3)
$La_{1.4}Nd_{0.6}RuO_5$	135	182	219	330	564	4.0(3)
$La_{1.6}Sm_{0.4}RuO_5$	139	177	223	341	547	3.8(3)
$La_{1.7}Gd_{0.3}RuO_5$	140	192	231	358	583	4.0(3)
$La_{1.8}Dy_{0.2}RuO_5$	140	192	238	354	580	3.6(3)

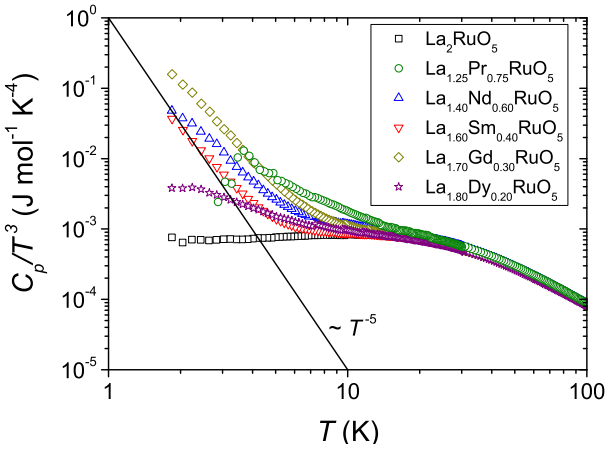

Fig. 3. (Color online) Low temperature specific heat on a double logarithmic scale in the representation C_p/T^3 vs. T of La_2RuO_5 and selected $La_{2-x}Ln_xRuO_5$ samples.

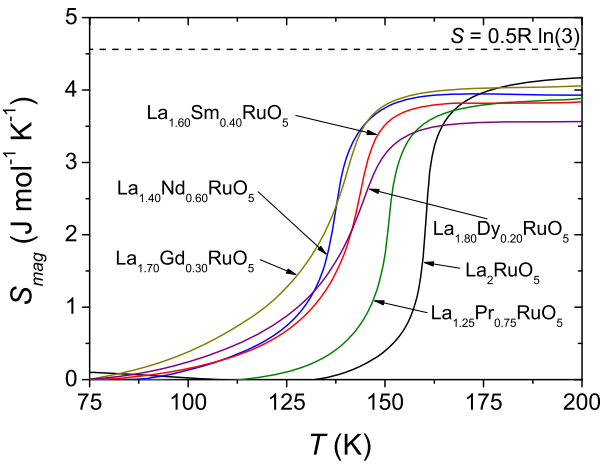

Fig. 4. (Color online) Magnetic entropy obtained from integration of the $La_{2-x}Ln_xRuO_5$ specific heat residuals after subtraction of the lattice contribution. The value of 0.5R ln(3) is a first approximation showing the significant contribution of the dimer state to the total entropy.

appear to be weaker in this temperature range. Measurements in different magnetic fields yield behaviors consistent with Schottky-type anomalies. The appearance of an uprise for $La_{1.7}Gd_{0.3}RuO_5$ was rather surprising with respect to its intensity, but is in agreement with similar findings for e.g. $Gd_{1-x}Sr_xTiO_3$ [26]. As expected, for the pure La_2RuO_5 no significant increase of C_p is observed.

Using a single Debye T^3 term for the low temperature region, a first estimate of the Debye temperature of La_2RuO_5 was obtained. The resulting temperature of 251 K is in very good agreement with 255 K reported by Malik et al. [15]. As can be seen from Figure 3 this simplified model is not suitable to describe the specific heat due to the temperature dependent behavior of C_p/T^3. For the more sophisticated Einstein-Debye fit of C_p/T an additional term c_0 was required to improve the fit quality. The obtained value $c_0 = 2.2$ mJ mol^{-1} K^{-2} for La_2RuO_5 is slightly larger than the value reported in literature (0.78 mJ mol^{-1} K^{-2}) [15]. In metals c_0 is known as Sommerfeld-coefficient representing the contribution of the conduction electrons, which is proportional to the density of states at the Fermi energy. For semiconducting oxides, however, a value of zero is expected because of the band gap. Here c_0 is only a parameter which, on the one hand, is neccessary due to the strong constraints made with respect to the phonon parameters and, on the other hand accounts for any additional temperature-independent contribution to the specific heat like e.g. the higher crystal field levels of the rare-earth ions which can extend up to energies corresponding to room temperature. These contributions will not be further discussed due to their complexity in oxide materials.

In Figure 2 the Einstein-Debye fit results are shown as solid lines and they are in good agreement with the measured data (symbols). This adequate description of the phonon contribution is required for reliable results since even small deviations strongly influence the subsequent calculations. To obtain the magnetic contribution to C_p, the Einstein-Debye fits (parameters in Tab. 1) were subtracted from the experimental data. The residuals $C_p - C_{lattice}$ were integrated between approximately 75 K and 250 K according to $S_{mag} = \int (C_p - C_{lattice})/T \mathrm{d}T$. The results for the entropies S_{mag} are depicted in Figure 4 and show very similar constant excess entropies between 3.6 and 4.2 J mol^{-1} K^{-1} (Tab. 1) for all samples. These values corroborate the pure spin dimerization occurring at the magnetic transition and they are ruling out any kind of long-range order in agreement with neutron diffraction experiments, in which no additional magnetic peaks were observed [14].

A magnetic entropy of $S_{mag} = \mathrm{R}\ln(2S+1) = 9.13$ J mol^{-1} K^{-1} is expected for the antiferromagnetic ordering of $S = 1$ spins. Values of 8.3 J mol^{-1} K^{-1} [15] and 8.56 J mol^{-1} K^{-1} [27] were reported in literature

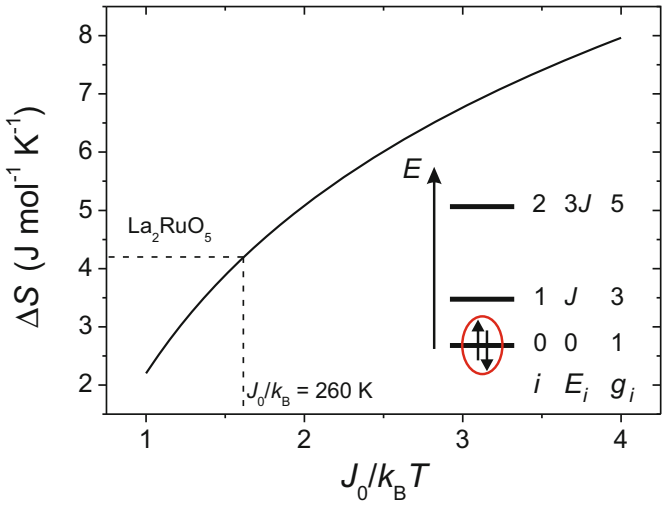

Fig. 5. (Color online) Entropy change ΔS depending on the intradimer exchange $J_0/k_\mathrm{B}T$ of La_2RuO_5 at T_d. Inset: energy level scheme of the dimer state consisting of $S = 1$ spins.

for La_2RuO_5 but rather simple approaches were used to model the lattice contributions. The Einstein-Debye fit applied in this work is more sophisticated and we believe that our smaller values are more reliable. The large deviation of the experimentally found and the expected value can be explained taking into account the lt-phase spin pairing. The molar entropy is defined as $S_{mag} = k_\mathrm{B}\ln(\Omega)$, where k_B is the Boltzmann constant and Ω is the partition function. In the lt-phase the entropy is deviating from zero due to the dimerization. The entropy change at T_d is therefore calculated according to $\Delta S = |\mathrm{R}\ln(3) - 0.5S_{dimer}|$ (see Fig. 5). The latter term represents the entropy of the dimers according to $S_{dimer} = \bar{E}/T + k_\mathrm{B}\ln(Z)$ and is multiplied by 0.5 due to the half number of dimers compared to the single spins. Z is the partition function of the energy spectrum of the dimers with a singlet ground state which is shown as inset in Figure 5. The first and second excited state of the dimers are a triplet and a quintuplet state, respectively. At T_d the partition function Z of this spectrum is given by:

$$Z = \sum_i g_i \exp\left(-\frac{E_i}{k_\mathrm{B}T_d}\right), \qquad (1)$$

where g_i is the degeneracy and E_i the energy of the corresponding state with respect to the ground state ($i = 0$). The averaged energy $\bar{E}$ of the spectrum is calculated according to:

$$\bar{E} = \frac{\sum_i g_i E_i \exp\left(-\frac{E_i}{k_\mathrm{B}T_d}\right)}{\sum_i g_i \exp\left(-\frac{E_i}{k_\mathrm{B}T_d}\right)}. \qquad (2)$$

The energies E_i in the spectrum in first approximation are determined by the intradimer exchange J_0 and therefore the entropy change is depending on the ratio of J_0 and the dimerization temperature T_d leading to the simplified averaged energy for the dimer state:

$$\bar{E}_{dimer} = \frac{3J_0}{k_\mathrm{B}} \frac{\exp\left(-\frac{J_0}{k_\mathrm{B}T_d}\right) + 5\exp\left(-\frac{3J_0}{k_\mathrm{B}T_d}\right)}{1 + 3\exp\left(-\frac{J_0}{k_\mathrm{B}T_d}\right) + 5\exp\left(-\frac{3J_0}{k_\mathrm{B}T_d}\right)}. \qquad (3)$$

Using these equations the entropy change can be calculated with respect to $J_0/k_\mathrm{B}T_d$ which is depicted as solid black line in Figure 5. The obtained value of 4.2 $\mathrm{J\,mol^{-1}\,K^{-1}}$ for pure La_2RuO_5 (marked by the dashed lines) corresponds to an intradimer exchange of $J_0/k_\mathrm{B} \approx 260$ K (23.5 meV) which is smaller than the 40 meV obtained by inelastic neutron scattering. By DFT calculations a value of 65.5 meV was derived, which is somewhat larger but still in the same range as our finding [6,10]. 23.5 meV is a lower estimate of the exchange since the interactions between the dimers are neglected in our model.

The very similar values obtained for S_{mag} reveal the same nature of the phase transitions and spin dimerization in all $La_{2-x}Ln_xRuO_5$ compounds in agreement with the results described in the following section. Furthermore, the slight variation of the entropies correlates to some extend with the varying dimerization temperatures of the rare-earth substituted samples reflecting a slightly reduced intradimer exchange J_0 as a result of the substitution [8].

On the other hand, besides the magnetic entropy, also the effect of the structural transition has to be regarded. However, it is impossible to separate its contribution since both transitions are coupled. The above described good agreement of the magnetic entropy with the theoretical estimate indicates that the change of C_p caused by the structural transition is very small.

3.2 Magnetic susceptibility

In a preceeding publication we were able to describe the magnetic data of $La_{2-x}Ln_xRuO_5$ above the transtition temperature by the sum of the magnetic moments of Ru^{4+} ions ($S = 1$) and trivalent rare-earth ions [8]. Here, the discussion of the magnetic behavior is extended to the low-temperature region, i.e. temperatures below the phase transition.

To investigate the magnetic behavior of $La_{2-x}Ln_xRuO_5$ in the lt-phase, the experimental susceptibilities were evaluated with respect to the rare-earth contribution by subtracting the susceptibility of unsubstituted La_2RuO_5. The residuals were fitted with the sum of a Curie-Weiss law and a constant contribution $\chi = C/(T - \Theta_{CW,Ln}) + \chi_0$ in the temperature interval 10 K $\leq T \leq$ 300 K. Very small χ_0 values in the order of 10^{-4} emu/mol were obtained which are in the range of the observed temperature independent shifts visible in Figures 6 and 7. The χ_0 values will be discussed in more detail below. Applying the free-ion approximation [28], the expected values for the rare-earth moments are $n_{\mathrm{eff,theo}} = \sqrt{x}\, n_{\mathrm{eff},Ln}$. In Table 2 the experimentally obtained ($n_{\mathrm{eff,fit}}$) and expected ($n_{\mathrm{eff,theo}}$) values are listed for the compounds with substitution level $x = 0.1$ and for

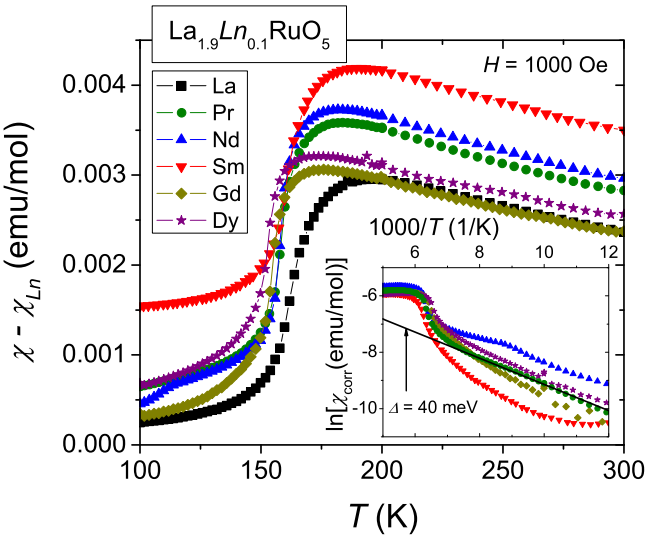

Fig. 6. (Color online) Temperature dependence of the magnetic susceptibility of La_2RuO_5 and $La_{1.9}Ln_{0.1}RuO_5$ after subtraction of the corresponding trivalent rare-earth susceptibility χ_{Ln}. The inset shows Arrhenius-plots of the additionally χ_0-corrected susceptibilities χ_{corr}. The solid black line corresponds to a 40 meV spin-gap.

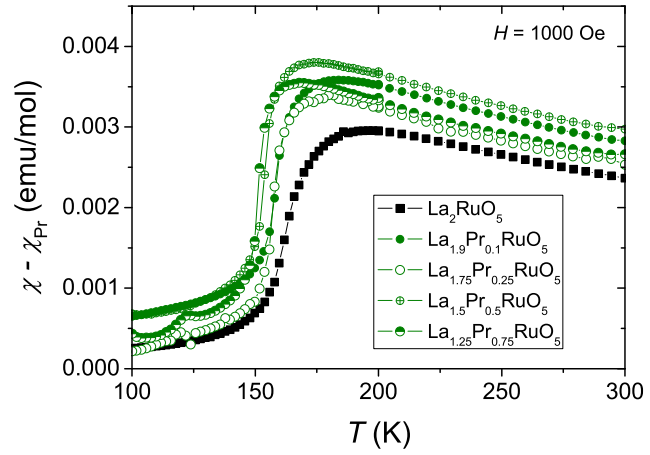

Fig. 7. (Color online) Temperature dependence of the magnetic susceptibility of La_2RuO_5 and $La_{2-x}Pr_xRuO_5$ after subtraction of the Pr^{3+} susceptibility χ_{Pr}.

selected Pr substituted compounds (x = 0.25, 0.5, 0.75). The results for $n_{\mathrm{eff,fit}}$ are in reasonable agreement with the expected values. On the one hand this reflects the correct stoichiometry of rare-earth ions in the compounds and on the other hand it also proves that the summation of the rare earth and the Ru magnetic moment is a reasonable approximation to describe the magnetic behavior of the samples, both below and above the magnetic transition. Only at temperatures below roughly 30 K this model cannot be applied, because crystal-field effects and interactions between the $4f$ electrons of the rare-earth ions become important. This effect correlates with the specific-heat data described above. The Curie-Weiss temperatures $\Theta_{CW,Ln}$ are close to zero for most of the

Table 2. Effective magnetic moments n_{eff} and Curie-Weiss temperatures $\Theta_{CW,Ln}$ of the Ln^{3+} ions in selected $La_{2-x}Ln_xRuO_5$ compounds. See text for details.

Compound	$\Theta_{CW,Ln}$ (K)	$n_{\mathrm{eff,fit}}$ (μ_B)	$n_{\mathrm{eff,theo}}$ (μ_B)
$La_{1.9}Sm_{0.1}RuO_5$	–3.61(5)	0.27(2)	0.26
$La_{1.9}Nd_{0.1}RuO_5$	0.19(5)	0.81(2)	1.14
$La_{1.9}Gd_{0.1}RuO_5$	–0.08(5)	2.44(2)	2.50
$La_{1.9}Dy_{0.1}RuO_5$	–0.24(5)	3.05(2)	3.36
$La_{1.9}Pr_{0.1}RuO_5$	–3.74(5)	1.03(2)	1.13
$La_{1.75}Pr_{0.25}RuO_5$	–6.71(5)	1.60(2)	1.78
$La_{1.5}Pr_{0.5}RuO_5$	–7.10(6)	2.34(2)	2.53
$La_{1.25}Pr_{0.75}RuO_5$	–16.63(8)	3.03(2)	3.09

samples, indicating a negligible magnetic interaction of the rare-earth ions. In the Pr-doped compounds slightly negative, $\Theta_{CW,Ln}$ values are caused by the crystal-field splitting of the Pr ground state [29].

In Figures 6 and 7, modified susceptibilities for $La_{1.9}Ln_{0.1}RuO_5$ and $La_{2-x}Pr_xRuO_5$ are depicted. To derive these curves the contribution of the rare-earth ions was calculated using n_{eff} and $\Theta_{CW,Ln}$ from Table 2 and subtracted from the experimental data. The results are denoted in the following as $\chi - \chi_{Ln}$ and $\chi - \chi_{\mathrm{Pr}}$, respectively. The susceptibility of pure La_2RuO_5 is shown in both figures for comparison. The remaining susceptibilities for $La_{2-x}Ln_xRuO_5$ are very similar to the one of La_2RuO_5. Especially the strongly reduced low-temperature susceptibility and the transition step between 150 K and 170 K are clearly visible for all compounds. Also the shift of the transition temperatures depending on the rare-earth element and the substitution level x is evident [8]. The values of $\chi - \chi_{Ln}$ above the magnetic transition change in the order Sm > Nd, Pr > Dy, Gd ≥ La_2RuO_5. This temperature independent shifts can partly be explained by the van-Vleck paramagnetism χ_0 of the rare-earth ions which is here unexpectedly strong for Sm, intermediate for Nd and Pr, and negligible for Gd and Dy according to the crystal-field multiplet-level splitting [28].

The derivatives of the susceptibilities yield a peak which can be fitted using a Lorentzian profile as shown in reference [12]. The temperatures of the peak centers are in good agreement with the transition temperatures reported in reference [8], but are shifted to lower temperatures by approximately 4 K. This is to be expected since in reference [8] the onset temperatures were used. The full widths at half maximum of the peaks vary between 6 K and 10 K and the peak areas remain almost constant for all samples reflecting the identical spin-dimerization occurring in the samples.

To investigate the size of the spin-gaps, χ_0 is additionally subtracted from the susceptibilities and the residuals are denoted as χ_{corr}. In the inset of Figure 6 the logarithm $\ln[\chi_{corr}]$ is depicted as a function of the inverse temperature in an Arrhenius-plot providing spin-gaps of 40 ± 10 meV for the samples with $x = 0.1$. This constant value is also found for the Pr substitution series and therefore it can be concluded that a constant spin-gap of roughly 40 meV is characteristic for all polycrystalline

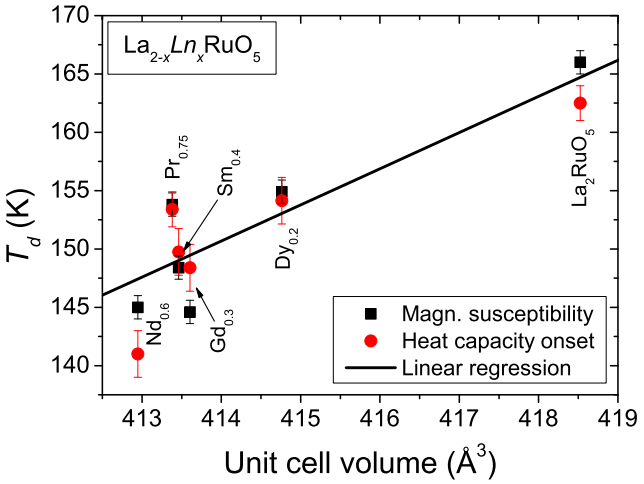

Fig. 8. (Color online) Transition temperatures T_d for $La_{2-x}Ln_xRuO_5$ (denoted as Ln_x) obtained from the onset of the inverse magnetic susceptibility (squares) and from heat capacity (circles) as a function of the unit-cell volume. The solid black line represents a linear regression.

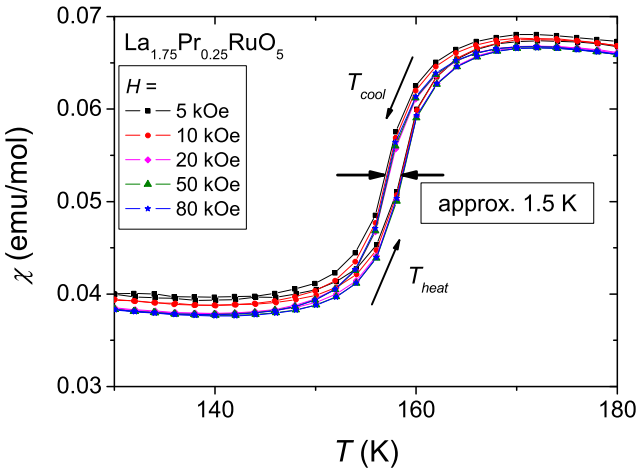

Fig. 9. (Color online) Temperature dependent magnetic susceptibility of $La_{1.75}Pr_{0.25}RuO_5$ for different external magnetic fields. Cooling and heating cycles are marked by arrows.

La_2RuO_5 samples. This indicates that the the rare-earth substitution has only a negligible influence on the spin-gap in accordance with the weak influence of the lanthanides on the physical properties and crystal structure [8]. Furthermore, the almost constant spin-gaps are behaving similar to the related J_0 values obtained from the peak in the specific heat.

The dimerization temperatures T_d obtained from magnetic susceptibility measurements can be compared to the temperatures determined by heat-capacity measurements. For both methods the onset values were determined as described in reference [8]. In Figure 8 the results from both methods are depicted as a function of the unit cell volume. The black line reflects the linear relation of transition temperature and structural changes. Within the 2σ limit identical values for the transition temperatures were found by magnetic and specific-heat measurements. In addition very similar onset temperatures were obtained from differential scanning calorimetry measurements [8]. The transition temperature variation vs. the unit cell volume illustrates the strong correlation between the structural changes and the spin-dimerization temperatures. Furthermore, the good agreement of T_d obtained from magnetic and heat-capacity measurements shows that the C_p anomalies are indeed resulting from the Ru spin-dimerization.

To summarize, the results reported so far reveal that almost independent magnetic sublattices exist in both the ht- and the lt-modification. The magnetic susceptibility can conclusively be described by a sum of the paramagnetic rare-earth contribution and the La_2RuO_5 susceptibility. Similar independent magnetic sublattices were also observed in other perovskite related oxides like e.g. $Ln_{2/3}Cu_3Ti_4O_{12}$, where the antiferromagnetic ordering of the Cu^{2+} ions at roughly 25 K is not influenced by the additional paramagnetic rare-earth moments [30].

As reported in reference [12], the change in the susceptibility takes place in a very narrow temperature interval for single crystals of La_2RuO_5 and exhibits a thermal hysteresis of roughly 4 K. For polycrystalline samples, on the other hand, the transition is broadened to a range of roughly 30 K without a visible hysteresis. This large temperature interval can be explained by minor local inhomogeneities in the polycrystalline material. Since no broadening of the X-ray or neutron-diffraction peaks was observed, the proposed inhomogeneities must be limited to a very local scale. This interpretation is supported by the fact that a La_2RuO_5 sample synthesized by solid-state reaction with 24 hours calcination [14] showed a broader transition compared to the sample prepared by the soft chemistry route. It can be seen in Figures 6 and 7 that the lanthanide substitution does not additionally change the width of the transition step which is in agreement with the above described independency of the magnetic sublattices and the identical sample morphology expected for the sol-gel prepared samples.

The occurrence of a possible transition hysteresis in the $La_{2-x}Ln_xRuO_5$ samples was studied, and as an example, Figure 9 shows temperature cycles of the susceptibility of $La_{1.75}Pr_{0.25}RuO_5$ for various magnetic fields between $H = 5$ kOe and 80 kOe. The difference between the heating and cooling curves amounts to roughly 1.5 K which is comparable to the difference obtained by differential scanning calorimetric measurements [8]. For the other compounds similar values were obtained; in most cases the temperature deviation was well below 1 K. Although in La_2RuO_5 single crystals the hysteresis of 4 K suggests a first order character, the broadening of the transition due to inhomogeneities in the polycrystalline samples induces a more second order like behavior.

3.3 Band-structure calculations

Previous DFT calculations by Eyert et al. [16,17] and Wu et al. [10] revealed a spin-Peierls like transition in

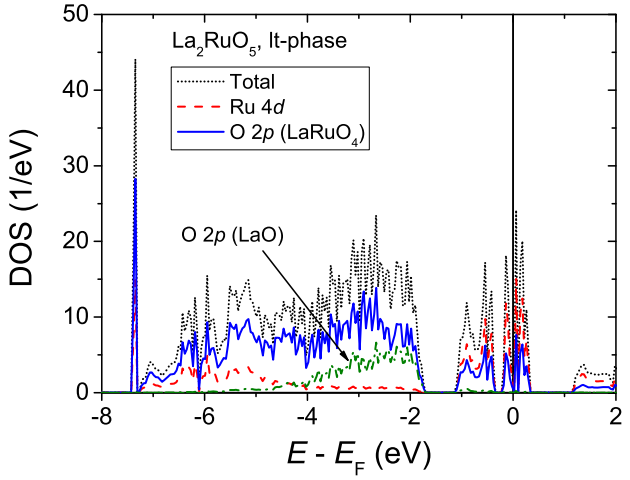

Fig. 10. (Color online) Density of states (DOS) of the spin-up channel (LSDA) for the lt-phase of La_2RuO_5.

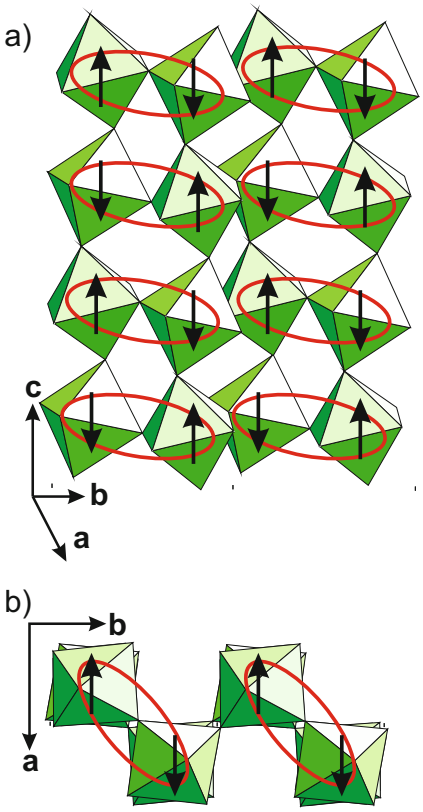

Fig. 11. (Color online) Ru-spin ordering in the lt-phase of La_2RuO_5. RuO_6 octahedra of the $LaRuO_4$ double layer are drawn within a $2\times2\times2$-unit cell. Rare earth ions are not shown for clarity. Black arrows indicate the $S = \pm1$ spin arrangement of the Ru^{4+}-ions, but do not represent an absolute orientation. The Ru–Ru singlets are indicated by red ellipses; a) perspective viewing, b) projection along the c-axis.

La_2RuO_5 conserving the local $S = 1$ spin-moment of the Ru^{4+} ions. According to these calculations, the drastically lowered magnetic susceptibility of the lt-modification is caused by an antiferromagnetic coupling of neighboring Ru ions which is cancelling out the net magnetic moment, resulting in a non-magnetic singlet ground state. This transition was reported to result from changes in the electronic structure initialized by structural modifications driven by an orbital ordering process of the Ru $4d$ orbitals [6]. Recently we have shown that due to the deformation of the RuO_6 octahedra already the ht-phase yields a splitting of the $4d$ t_{2g} orbitals, which is stabilized in the lt-phase by the structural changes occuring at T_d [21]. As a consequence of these changes the exchange interaction between neighboring Ru spins favors the formation of Ru spin-singlets with the observed reduced net magnetic moment.

Here we report on DFT calculations applying the spin-polarized LSDA. To assure the consistency of our calculations with previous investigations, the already published results for the ht- and lt-phase of La_2RuO_5 according to references [16,17] were reproduced in a first step by the FPLO code[3]. The results for the unpolarized modelling (LDA) of the La_2RuO_5 ht-phase are not shown since they are very similar to the previously published data [16,17]. Spin-polarized modelling (LSDA) of the ht-phase revealed an antiferromagnetic interaction of the Ru spins which is in agreement with the negative Curie-Weiss temperature of roughly −170 K.

In Figure 10 the DOS for the lt-phase of La_2RuO_5 is depicted in the interval –8 eV to 2 eV around the Fermi-energy (E_F). The DOS is in reasonable accordance with literature [16,17]. In particular, we found the same contribution of Ru $4d$ and O $2p$ orbitals around E_F. The oxygen contribution in this range explicitely stems from the RuO_6 octahedra in the $LaRuO_4$-layers. The O $2p$ bands from the LaO-layers are found in the range –2 to –4 eV and show an increased negative valence compared to the other oxygen ions. This finding is consistent with bond valence sum calculations described in reference [8]. The contributions of the La orbitals are negligible in the energy range shown in Figure 10. The unoccupied La $4f$ bands are located roughly 4 eV above E_F.

For the lt-modification of La_2RuO_5 completely antiferromagnetically arranged Ru-spin moments were found. This ordered arrangement is energetically favored by roughly 10 meV compared to the unpolarized LDA model. Different spin arrangements were tried out as starting points. The corresponding calculations all lead to the same ordering scheme and therefore corroborate the energetic stability of this result. The obtained arrangement of the Ru spins is depicted schematically in Figure 11. To increase clarity only the RuO_6 zig-zag-like octahedra double layer of the $LaRuO_4$-unit is shown. Black arrows represent the Ru^{4+} spin moments with spin-up and spin-down orientation. It should be noted that the depicted directions are only the relative orientation of the spins with respect to each other and do not represent an absolute orientation with respect to the crystallographic axes. Figure 11a illustrates the antiferromagnetical Ru-spin pairing marked by red ellipses. In a projection along the c-axis the spatial

[3] Both the original symmetry as well as the reduction to P1 lead to almost identical results of the DFT calculations.

separation of the singlets in b-direction can be better recognized (see Fig. 11b). In addition, an antiferromagnetic arrangement of the Ru spin moments in the c-direction was revealed, which was not described in literature yet. In conclusion all Ru moments can be considered fully antiferromagnetically arranged to each neighboring Ru ion without any geometric frustration. This is also in agreement with the so-called frustration index, i.e. the ratio of the Curie-Weiss temperature and the dimerization temperature $|\Theta_{CW}/T_d|$, which were found to be close to unity [8].

The total antiferromagnetic spin arrangement seems to contradict the above-described negligible interaction between the individual dimers. It should be kept in mind, though, that the modelling results represent projections of the ground state populations for zero K. It is more reasonable to assume that at finite temperatures only significantly strong interactions will result in ordering phenomena, while very weak ones are broken up by thermal fluctuations. In earlier calculations it was shown that the interaction inside the rungs of the spin-ladders is strongest, followed by the interaction strength along the c-axis which are more than one order of magnitude weaker. The interladder coupling is even smaller [10]. From these different interaction strengths it can be concluded that only the antiferromagnetic spin-dimer coupling leads to an ordered state, while the interaction between different dimers is too weak to form a completely (pseudo-) 2D or 3D ordering. This interpretation reflects the above-described almost independent spin-dimers in the lt-singlet state derived from the C_p measurements and entropy analysis.

A comparison of the Ru contribution to the DOS close to E_F for different Pr substitution levels in the lt-phase of $La_{2-x}Pr_xRuO_5$ is shown in Figure 12. As can be seen, the Ru 4d bands are broadening and slightly shifting with increasing Pr content. The decreasing absolute values of the Ru spin moments correlate with the declining transition temperature in $La_{2-x}Ln_xRuO_5$ with increasing x [8]. In contrast, the DOS below $E_F - 2$ eV remains almost unchanged since the structural changes are barely influencing the oxgen 2p bands. As expected, the 4f states of Pr are located around the Fermi-energy in very narrow bands, however, the hybridization with the other bands seems to be negigible.

For all lt-modifications different starting models for the magnetic ordering and the Pr substitution were used. The completely antiferromagnetic arrangement shown in Figure 11 is slightly favored by up to 0.14 eV per unit cell for the Pr substituted compounds, compared to the unpolarized LDA calculations or the LSDA results obtained for other magnetic arrangements, independent of the magnetic moments of the Pr ions. The obtained local Ru spin-moments in the favored magnetic arrangment were found to be approximately $S_\uparrow = +0.95$ and $S_\downarrow = -0.98$ for neighboring sites in La_2RuO_5, reflecting the antiferromagnetic pairing. The absolute values of the localized moments are strongly decreasing with increasing Pr substitution level, mirroring a possible higher delocalization of the Ru spin moments which explains the

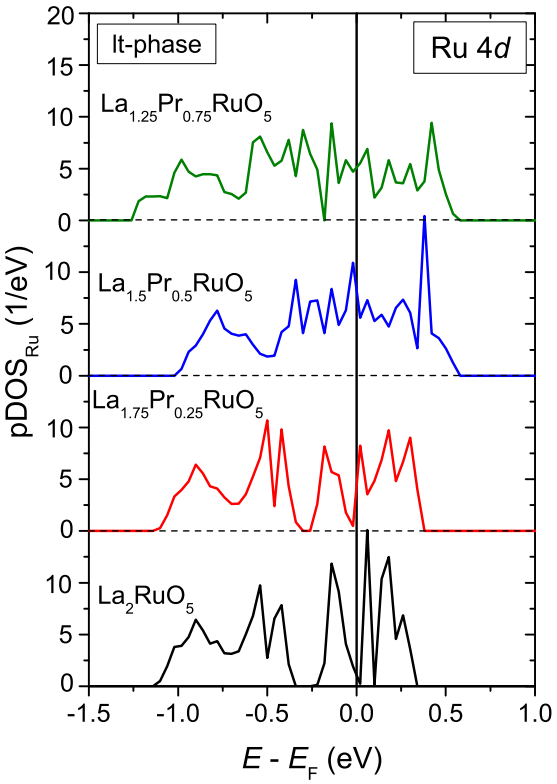

Fig. 12. (Color online) Sum of the Ru contributions (spin-up channel) to the partial density of states (pDOS) close to E_F in the lt-phase of selected $La_{2-x}Pr_xRuO_5$ compounds applying LSDA.

observed change in transition temperature[4]. For $x = 0.25$ spin moments, $+0.85$ and -0.79 are found, for $x = 0.50$ they amount to ± 0.32 and for $x = 0.75$ only $+0.05$ and -0.07 remain. This evolution of the absolute values of the local magnetic Ru moments at first sight seems to contradict the above described similar magnetic pairing in all rare-earth substituted compounds. However, the dimerization character is preserved by constant exchange interactions although the local magnetic moments distinctly decrease.

4 Summary and conclusions

In this work the magnetic phase transition in $La_{2-x}Ln_xRuO_5$ was studied regarding structural, magnetic and thermal properties with supporting DFT calculations.

The specific heat of selected $La_{2-x}Ln_xRuO_5$ samples and pure La_2RuO_5 was investigated. The lattice contribution to C_p was fitted using an Einstein-Debye model and subtracted from the experimental data. $(C_p - C_{lattice})/T$ was integrated over the temperature to obtain the magnetic entropy which was found to be nearly identical for all investigated compounds. The average entropy of roughly 3.9 $J\,mol^{-1}\,K^{-1}$ is significantly smaller

[4] Alternatively, this could be an artifact of the modelling. Possibly a part the Ru 4d electron density is simply shifted into the Pr 4f bands located at E_F.

than expected for the transition into an antiferromagnetically ordered system. This value can be explained taking into account the entropy of a spin-dimer lt-state consisting of $S = 1$ spins. By this model a lower estimate of the intradimer exchange of $J_0/k_B \approx 260$ K can be obtained from the experimental entropy which is almost constant for all investigated samples. For the lanthanide substituted samples the C_p/T peak broadens and shows a temperature shift in agreement with results obtained from magnetic susceptibility and differential scanning calorimetry measurements [8]. The peak broadening of C_p at the transition temperature very likely results from local inhomogeneities affecting the rare-earth substitution distribution.

For both the ht- and lt-phase of $La_{2-x}Ln_xRuO_5$ the magnetic susceptibility can be described by a sum of the contribution of the rare-earth ions and the susceptibility measured for unsubstituted La_2RuO_5. The spin pairing process reported for La_2RuO_5 is found for all $La_{2-x}Ln_xRuO_5$ compounds in agreement with the very similar magnetic entropies obtained from specific-heat measurements.

Spin polarized DFT calculations reveal a complete antiferromagnetic ordering of the Ru spin moments in the lt-modification of La_2RuO_5. Also in the ht-phase antiferromagnetic interactions are energetically favored, however the increased thermal fluctuations impede ordering. These results are in agreement with previous publications and the absence of geometrical frustration derived from magnetic susceptibility measurements. The DFT calculations for Pr substituted compounds using LSDA indicate that the magnetic moment of the Pr ions has only a minor influence on the magnetic ordering. The broadening of the Ru-bands close to E_F with increasing Pr substitution level in the lt-phase explains the lowering of the transition temperature by increasing delocalization of the Ru spin moments in agreement with earlier results [8]. Thus all experimentally observed features and the performed spin polarized DFT calculations tell us about the spin-singlet formation in the lt-phase of $La_{2-x}Ln_xRuO_5$ with a quite large exchange coupling parameter $J_0/k_B \approx 260$ K (23.5 meV).

The authors gratefully thank E.-W. Scheidt for providing the C_p-fit program and helpful discussion. Special thanks are due to Volker Eyert for his help in the interpretation of the DFT calculation. This work was supported by the DFG within the collaborative research unit TRR 80 (Augsburg, Munich).

References

1. S.J. Makowski, J.A. Rodgers, P.F. Henry, J.P. Attfield, J.-W.G. Bos, Chem. Mater. **21**, 264 (2009)
2. Z.H. Han, H.E. Mohottala, J.I. Budnick, W.A. Hines, P.W. Klamut, B. Dabrowski, M. Maxwell, J. Phys.: Condens. Matter **18**, 2273 (2006)
3. J.A. Rodgers, P.D. Battle, C.P. Grey, J. Sloan, Chem. Mater. **17**, 4362 (2005)
4. W.G. Mumme, A.D. Wadsley, Acta Cryst. B **24**, 1327 (1968)
5. G. Cao, S. McCall, Z.X. Zhou, C.S. Alexander, J.E. Crow, R.P. Guertin, C.H. Mielke, Phys. Rev. B **63**, 144427 (2001)
6. P. Khalifah, R. Osborn, Q. Huang, H.W. Zandbergen, R. Jin, Y. Liu, D. Mandrus, R.J. Cava, Science **297**, 2237 (2002)
7. S.G. Ebbinghaus, S. Riegg, T. Götzfried, A. Reller, Eur. Phys. J. ST **180**, 91 (2010)
8. S. Riegg, U. Sazama, M. Fröba, A. Reller, S.G. Ebbinghaus, Phys. Rev. B **84**, 014403 (2011)
9. D.I. Khomskii, T. Mizokawa, Phys. Rev. Lett. **94**, 156402 (2005)
10. H. Wu, Z. Hu, T. Burnus, J.D. Denlinger, P.G. Khalifah, D.G. Mandrus, L.-Y. Jang, H.H. Hsieh, A. Tanaka, K.S. Liang, J.W. Allen, R.J. Cava, D.I. Khomskii, L.H. Tjeng, Phys. Rev. Lett. **96**, 256402 (2006)
11. S.J. Moon, W.S. Choi, S.J. Kim, Y.S. Lee, P.G. Khalifah, D. Mandrus, T.W. Noh, Phys. Rev. Lett. **100**, 116404 (2008)
12. S. Riegg, A. Günther, H.-A. Krug von Nidda, A. Loidl, M.V. Eremin, A. Reller, S.G. Ebbinghaus, Phys. Rev. B **86**, 115125 (2012)
13. P. Boullay, D. Mercurio, A. Bencan, A. Meden, G. Drazic, M. Kosec, J. Solid State Chem. **170**, 294 (2003)
14. S.G. Ebbinghaus, Acta Cryst. C **61**, i96 (2005)
15. S.K. Malik, D.C. Kundaliya, R.D. Kale, Solid State Commun. **135**, 166 (2005)
16. V. Eyert, S.G. Ebbinghaus, T. Kopp, Phys. Rev. Lett. **96**, 256401 (2006)
17. V. Eyert, S.G. Ebbinghaus, Prog. Solid State Chem. **35**, 433 (2007)
18. E.C. Samulon, M.C. Shapiro, I.R. Fisher, Phys. Rev. B **84**, 054417 (2011)
19. K. Koepernick, H. Eschrig, Phys. Rev. B **59**, 1743 (1999)
20. I. Opahle, K. Koepernick, H. Eschrig, Phys. Rev. B **60**, 14035 (1999)
21. S. Riegg, A. Reller, S.G. Ebbinghaus, J. Solid State Chem. **188**, 17 (2012)
22. R.P. Singh, C.V. Tomy, J. Phys.: Condens. Matter **20**, 235209 (2008)
23. C. Kant, J. Deisenhofer, A. Günther, F. Schrettle, A. Loidl, M. Rotter, D. Johrendt, Phys. Rev. B **81**, 014529 (2010)
24. S. Layek, V.K. Anand, Z. Hossain, J. Magn. Magn. Mater **321**, 3447 (2009)
25. A. Tari, *The specific heat of matter at low temperatures* (Imperial College Press, London, 2003)
26. M. Heinrich, H.-A. Krug von Nidda, V. Fritsch, A. Loidl, Phys. Rev. B **63**, 193103 (2001)
27. B. Rivas-Murias, H.D. Zhou, J. Rivas, F. Rivadulla, Phys. Rev. B **83**, 165131 (2011)
28. H. Lueken, *Magnetochemie* (Teubner, Stuttgart - Leipzig, 1999)
29. W.G. Penney, R. Schlapp, Phys. Rev. **41**, 194 (1932)
30. A. Dittl, S. Krohns, J. Sebald, F. Schrettle, M. Hemmida, H.-A. Krug von Nidda, S. Riegg, A. Reller, S.G. Ebbinghaus, A. Loidl, Eur. Phys. J. B **79**, 391 (2011)